

Computation of Polarized Subsurface BRDF for Rendering

Charly Collin*
EECS

University of Central Florida

Sumanta Pattanaik†
EECS

University of Central Florida

Patrick LiKamWa ‡
CREOL

University of Central Florida

Kadi Bouatouch §
IRISA

Université de Rennes 1

ABSTRACT

Interest in polarization properties of the rendered materials is growing, but so far discussions on polarization have been restricted only to surface reflection, and the reflection due to subsurface scattering is assumed to be unpolarized. Findings from other field (e.g. optics and atmospheric science) show that volumetric interaction of light can contribute to polarization. So we investigated the polarized nature of the radiance field due to subsurface scattering as a function of the thickness of the material layer for various types of materials. Though our computations shows negligible polarization for material layers of high thickness, thin layered materials show significant degree of polarization. That means polarization cannot be ignored for subsurface component of reflection from painted surfaces (particularly painted metal surfaces) or from coated materials. In this paper we employ the vector radiative transfer equation (VRTE), which is the polarized version of the radiative transfer equation inside the material. We use a discrete ordinate based method to solve the VRTE and compute the polarized radiance field at the surface of the material layer. We generate the polarimetric BRDF from the solutions of the VRTE for incident irradiance with different polarizations. We validate our VRTE solution against a benchmark and demonstrate our results through renderings using the computed BRDF.

Index Terms: I.3.0 [Computer Graphics]: General—; I.4.1 [Image Processing and Computer Vision]: Digitalization and Capture—Reflectance

1 INTRODUCTION

Accurate modeling of the bidirectional reflection distribution function (BRDF) of materials is important for realistic rendering. The BRDF of most real world materials is composed of two components: (a) the *surface* BRDF, the component due to surface only interaction of light, and (b) the *subsurface* BRDF, the component due to subsurface interaction of light as defined by Hanrahan and Krueger [6, 7]. Both of these components may have significant directional dependence. The Fresnel equation models the surface BRDF component for smooth surfaces and is often extended to rough surfaces by modeling the surface by a microfacet distribution [14]. Subsurface BRDF computation requires the simulation of light interaction inside the medium. Radiative transport equation (RTE) models this interaction [5]. Solution of RTE is expensive and is particularly so for BRDF computation. In the Computer Graphics literature, various approximation methods (for example: diffuse approximation [10]) have been proposed for computing this subsurface component. In this paper we use a discrete ordinate based solution method (DOM) of solving RTE for accurately computing the subsurface component of BRDF. Our simulations are done on

plane-parallel media composed of spherical or randomly oriented symmetric particles.

Light, as an electromagnetic wave, exhibits polarization. The human visual system cannot directly detect the polarization state of light, which is the reason why it is often omitted in rendering. However, the polarization state of light affects the interaction between light and matter, and hence must be taken into account for accurate global illumination computation [16, 18]. The Fresnel equation explicitly models polarization. So polarized surface reflection components have been used in global illumination computation. The subsurface interaction of light is assumed to create a randomly polarized (or unpolarized) radiation field, and consequently subsurface BRDF is assumed to be unpolarized as well. In this paper we use the vector radiative transport equation (VRTE) to simulate polarization effects due to subsurface interaction of light and to show that radiation field and BRDF due to subsurface interaction can be significantly polarized. We carry out an experiment and show the evidence for polarization in the subsurface component of BRDF. We solve VRTE to compute polarized subsurface BRDF for real world materials and use those in global illumination computation to show their effect on the polarization of a scene.

The organization of the paper is as follows. After a brief overview of Stokes vector representation of polarized light, and of RTE for modeling light transport in plane-parallel media, we introduce the vector radiative transfer equation (VRTE) to model the subsurface transport of polarized light and its discrete ordinate (DOM) based solution for subsurface BRDF computation. We validate our implementation of the DOM based VRTE solution method against a benchmark, and study the polarization property of the subsurface BRDF as a function of various parameters. We describe an experiment to verify the evidence of polarization in subsurface BRDF. Using our polarized path tracer, we show that polarized BRDF is important for accurate light transport in a scene, particularly so when polarizing reflectors or filters and/or polarizing source are present in the scene. Finally, we show some renderings to visualize the polarization components of the light transport in a scene.

2 BACKGROUND

2.1 Polarized light

Light polarization is explained by the electro-magnetic wave nature of light, and describes the orientation of the electric wave at any point in space. This wave may be oriented in a single direction perpendicular to the direction of propagation (linear polarization), or it may rotate as light propagates (circular polarization). Any propagated light may have a combination of these polarizations.

Among the possible formalisms describing the polarization state of light, Stokes vector [8] is a popular choice for its simplicity to understand and because its components are measurable. It is a four component vector:

$$\mathbf{I} = [I, Q, U, V]^t.$$

In this representation, I is the radiance and is exactly the same quantity that is used in the scalar representation. Q is the difference between the linearly polarized components of radiance along the horizontal and vertical axis, U is the difference of radiance between the linearly polarized components at 45 degrees and 135 degrees, and V is the difference of radiance between the right circularly and left

*e-mail: charly.collin@bobbyblues.com

†e-mail: sumant@cs.ucf.edu

‡e-mail: patrick@creol.ucf.edu

§e-mail: kadi@irisa.fr

circularly polarized components. The four components satisfy the following relation: $I^2 \geq Q^2 + U^2 + V^2$, and the degree of polarization (DOP) of light is expressed as:

$$DOP = \frac{\sqrt{Q^2 + U^2 + V^2}}{I}. \quad (1)$$

While I , the first component of the Stokes vector is always positive, the other three take their values in the range $[-I, I]$. For example, a Stokes vector with $V = -I$ represents light with full left circular polarization. For unpolarized light only the I component is non zero, and hence its Stokes vector representation is $[I, 0, 0, 0]^T$. In the rest of this paper we use symbols I and \mathbf{I} , to represent the scalar and vector forms of radiance respectively.

For simpler tracking of the orientation of the linear polarization, a Stokes vector is associated with a local reference frame (XYZ) whose Z-axis is defined along the propagation direction of the light and the other two axes are in a plane perpendicular to that direction. While the choice of the orientation of X,Y axes is arbitrary, it defines the components Q and U . When adding two Stokes vectors, one has to make sure that their reference frames are the same, which can be achieved through rotation. For two Stokes vectors whose X-axes (or Y-axes) are separated by an angle σ , the corresponding rotation matrix is:

$$Rotation(\sigma) = \begin{bmatrix} 1 & 0 & 0 & 0 \\ 0 & \cos 2\sigma & -\sin 2\sigma & 0 \\ 0 & \sin 2\sigma & \cos 2\sigma & 0 \\ 0 & 0 & 0 & 1 \end{bmatrix}. \quad (2)$$

Light-matter interaction (e.g. reflection or scattering) may have different effect on the radiance and the polarization. One element of the Stokes vector could increase while another one decrease for example. A single scalar factor is then not enough to represent those changes and a 4×4 matrix, called Mueller matrix, is used to describe such interactions [4]. That means the optical property of the matter must be specified by its characteristic Mueller matrix \mathbf{M} . Optical properties of particular importance to Computer Graphics are reflection and scattering, and both of those must be specified as Mueller matrix functions of incident and outgoing directions. A Mueller matrix is defined for incident and outgoing Stokes vectors with their specific reference frames. Changing the reference frame of any of those vectors changes the Mueller matrix as well. Therefore, given a Mueller matrix, one has to rotate carefully the incident and outgoing Stokes vector to match the desired reference frames. During the propagation of light its reflection or scattering is computed through multiplication between the Mueller matrix and the Stokes vector. We refer the reader to previous work [4, 19] for more details on Stokes vectors and Mueller matrix operations.

2.2 Radiative Transport Equation

The volumetric interaction of light is modeled by the radiative transfer equation (RTE) that expresses the radiance field in the medium as a function of the incident radiance. If we assume that the subsurface material volume is a plane-parallel medium, meaning that its scattering and absorption properties vary only along the depth (the direction perpendicular to the horizontal plane), then the radiance $I(\tau, \mu, \phi)$ in a non-emitting volume at an optical thickness τ along the direction (μ, ϕ) due to light incident (I_{inc}) from a single direction (μ_{inc}, ϕ_{inc}) (see Figure 1), is expressed by the RTE as follows:

$$\mu \frac{\partial}{\partial \tau} I(\tau, \mu, \phi) + I(\tau, \mu, \phi) - J(\tau, \mu, \phi) = Q(\tau, \mu, \phi), \quad (3)$$

where μ is the cosine of the outgoing direction's zenith angle and ϕ its azimuth angle. The function Q accounts for the radiance due

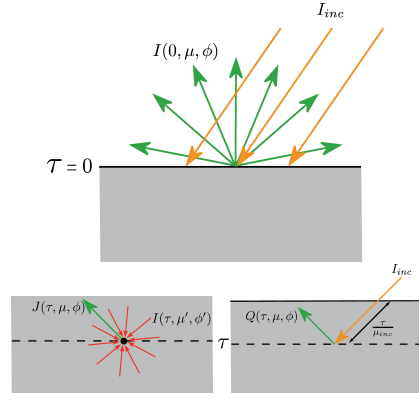


Figure 1: 2D cross section of a material composed of plane-parallel volume. The computation of the radiance at an optical thickness of τ in a direction (μ, ϕ) requires solving RTE in the volume.

to the direct scattering of I_{inc} (illustrated in the bottom right image of Figure 1) and is expressed as:

$$Q(\tau, \mu, \phi) = \frac{\omega(\tau)}{4\pi} Z(\tau, \mu, \mu_{inc}, \phi - \phi_{inc}) I_{inc}(\mu_{inc}, \phi_{inc}) e^{-\tau/\mu_{inc}}, \quad (4)$$

with ω as the single scattering albedo and Z as the phase function of the volume layer at the optical thickness τ . Note that the RTE used here is defined according to the optical thickness τ instead of the more classic euclidian distance. The optical thickness between two points x and x' is defined as:

$$\tau(x, x') = \int_x^{x'} \sigma_t(t) dt, \quad (5)$$

with σ_t being the extinction coefficient. In equations 3, 4 and 6 we assume that the medium is composed of spherical or randomly oriented particles and so the phase function is rotationally invariant. Moreover, because of the plane-parallel representation of the medium, we assume without loss of generality that the entering and exiting points of the light in and out the medium are the same. The function J in equation 3 accounts for the indirect radiance due to the multiple scattering of light (illustrated in the bottom left image of Figure 1) and is expressed as:

$$J(\tau, \mu, \phi) = \frac{\omega(\tau)}{4\pi} \int_0^1 \int_0^{2\pi} Z(\tau, \mu, \mu', \phi - \phi') I(\mu', \phi') d\phi' d\mu', \quad (6)$$

with (μ', ϕ') as the cosine zenith angle and azimuth angle of the in-scattering directions. Our goal in this paper is to compute and study the polarization properties of the radiance field due to subsurface interaction of the incident light, and compute polarized subsurface BRDF from this computed radiance field. In the next section we introduce VRTE, the extended RTE that supports polarization and discuss a solution method specific to this VRTE.

3 POLARIMETRIC SUBSURFACE BRDF AND ITS COMPUTATION

3.1 Vector RTE

In section 2 we described the Stokes vector representation \mathbf{I} for polarized radiance. We can write the RTE for this vector representation as[12]:

$$\mu \frac{\partial}{\partial \tau} \mathbf{I}(\tau, \mu, \phi) + \mathbf{I}(\tau, \mu, \phi) - \mathbf{J}(\tau, \mu, \phi) = \mathbf{Q}(\tau, \mu, \phi), \quad (7)$$

where \mathbf{J} and \mathbf{Q} are respectively the polarized components of the indirect and direct radiances and are expressed as:

$$\mathbf{J}(\tau, \mu, \phi) = \frac{\omega(\tau)}{4\pi} \int_0^1 \int_0^{2\pi} \mathbf{Z}(\tau, \mu, \mu', \phi - \phi') \mathbf{I}(\tau, \mu', \phi') d\phi' d\mu', \quad (8)$$

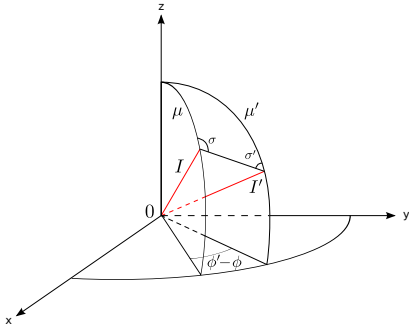


Figure 2: Main frame of reference and various angles.

$$\mathbf{Q}(\tau, \mu, \phi) = \frac{\omega(\tau)}{4\pi} \mathbf{Z}(\tau, \mu, \mu_{inc}, \phi - \phi_{inc}) \mathbf{I}_{inc}(\mu_{inc}, \phi_{inc}) e^{-\tau/\mu_{inc}}. \quad (9)$$

These equations are similar to their scalar counterpart and the Z phase function is replaced by the phase matrix \mathbf{Z} . We elaborate on the incident and scattered reference frames of \mathbf{I} and \mathbf{Z} in the next few paragraphs.

3.2 Reference frame of the Stokes Vector

As mentioned earlier, Stokes vectors are defined with respect to their reference frames. The reference frame that we use for solving the VRTE is described as follows. The Z axis of a ray's Stokes vector reference frame has to match its propagation direction (μ, ϕ) . We define both of this frame's X and Y directions in reference to the *meridional* or *meridian* plane, which is defined as the plane containing the light ray and the Z axis of the coordinate frame (see the vertical circular sectors in Figure 2 containing Z -axis of the world coordinate frame, and the ray direction vectors of the rays \mathbf{I} and \mathbf{I}'). The X axis of the reference frame lies in that plane while the Y axis is perpendicular to it such that XYZ forms a right handed coordinate system.

3.3 Scattering matrix

A scattering event in the volume scatters light in all direction around the point of interaction. The amount and the polarization of the scattered light is specified by the scattering matrix \mathbf{F} , which is a function of the scattering angle Θ between incident and scattered direction. Scattering depends on the size, shape and orientation of the interacting particles inside the volume of interaction, and in general all the 16 elements of the scattering matrix could be nonzero and each of the element is a scalar functions of Θ . As mentioned earlier, our discussion is restricted to the scattering of light inside volume composed of spherical or randomly oriented symmetric particles. As a consequence, the scattering matrix is rotationally invariant, and has eight non-zero elements, of which only six elements are unique [9].

$$\mathbf{F}(\Theta) = \begin{bmatrix} a_1(\Theta) & b_1(\Theta) & 0 & 0 \\ b_1(\Theta) & a_2(\Theta) & 0 & 0 \\ 0 & 0 & a_3(\Theta) & b_2(\Theta) \\ 0 & 0 & -b_2(\Theta) & a_4(\Theta) \end{bmatrix} \quad (10)$$

The phase functions are assumed to be normalized, that means:

$$\frac{1}{4\pi} \int_{\mathcal{S}^2} a_1(\Theta) d\omega = 1.$$

The elements in (10) may be tabulated for a discrete set of Θ values, or alternatively, may be expressed as coefficients of expansion in some orthogonal basis set.

Being a function of the scattering angle Θ only, the scattering matrix's reference frames are not expressed using the same rule as

in section 3.2. Instead, the local X -axes of the incident and outgoing directions of the scattering matrix lie in the scattering plane, the plane formed by the two directions (see Figure 2). So the X axis of the reference frames of both the incident and scattered ray must lie on that plane for the scattering matrix to be valid.

3.4 Phase matrix

For convenience, we would like our Mueller matrix for scattering to have the incident and scattered reflection frames to be the same as the reference frames of the incident Stokes vector and scattered Stokes vector. So instead of scattering matrix (\mathbf{F}) we use phase matrix (\mathbf{Z}) that has the latter property. Both matrices carry the same information (i.e. the amount of light scattered from incident direction to scattered direction), only their reference frames differ. Phase matrix is related to scattering matrix as:

$$\begin{aligned} \mathbf{Z}(\mu, \mu', (\phi - \phi')) &= \text{Rotation}(\pi - \sigma) \times \mathbf{F}(\Theta) \times \text{Rotation}(-\sigma') \\ &= \begin{bmatrix} 1 & 0 & 0 & 0 \\ 0 & \cos 2\sigma & \sin 2\sigma & 0 \\ 0 & -\sin 2\sigma & \cos 2\sigma & 0 \\ 0 & 0 & 0 & 1 \end{bmatrix} \\ &\quad \times \begin{bmatrix} a_1(\Theta) & b_1(\Theta) & 0 & 0 \\ b_1(\Theta) & a_2(\Theta) & 0 & 0 \\ 0 & 0 & a_3(\Theta) & b_2(\Theta) \\ 0 & 0 & -b_2(\Theta) & a_4(\Theta) \end{bmatrix} \\ &\quad \times \begin{bmatrix} 1 & 0 & 0 & 0 \\ 0 & \cos 2\sigma' & \sin 2\sigma' & 0 \\ 0 & -\sin 2\sigma' & \cos 2\sigma' & 0 \\ 0 & 0 & 0 & 1 \end{bmatrix}, \quad (11) \end{aligned}$$

where (μ', ϕ') and (μ, ϕ) represent the incident and scattered directions, σ' and σ are the angles between the scattering plane and the reference planes of incident Stokes vector and scattered Stokes vector respectively. See Figure 2 for the symbols.

Using spherical trigonometry, the scattering angle can be defined as

$$\cos \Theta = \mu' \mu + \sqrt{(1 - \mu'^2)(1 - \mu^2)} \cos(\phi - \phi'),$$

and the angles σ' and σ can be related to μ' , ϕ' , μ , ϕ as

$$\begin{aligned} \cos \sigma' &= \frac{\mu - \mu' \mu}{\sqrt{(1 - \mu'^2)} \sqrt{(1 - \cos^2 \Theta)}}, \\ \cos \sigma &= \frac{\mu' - \mu \cos \Theta}{\sqrt{(1 - \mu^2)} \sqrt{(1 - \cos^2 \Theta)}}. \quad (12) \end{aligned}$$

Finally, using simple trigonometric relations we can express $\cos 2\sigma$ and $\sin 2\sigma$ as:

$$\begin{aligned} \cos 2\sigma &= 2 \cos^2 \sigma - 1 \\ \sin 2\sigma &= \begin{cases} 2\sqrt{(1 - \cos^2 \sigma)} \cos \sigma & \text{for } 0 < \phi - \phi' < \pi \\ -2\sqrt{(1 - \cos^2 \sigma)} \cos \sigma & \text{otherwise.} \end{cases} \quad (13) \end{aligned}$$

3.5 Solution of the VRTE

Most numerical solution methods of RTE proceed by first removing the azimuthal dependency of the functions involved by expanding them in Fourier series. We expand the phase function in Fourier series as [12]:

$$\begin{aligned} \mathbf{Z}(\mu, \mu', \phi - \phi') &= \frac{1}{2} \mathbf{Z}^{c,0}(\mu, \mu') \\ &\quad + \sum_{m=1}^L (\mathbf{Z}^{c,m}(\mu, \mu') \cos[m(\phi - \phi')] + \mathbf{Z}^{s,m}(\mu, \mu') \sin[m(\phi - \phi')]), \quad (14) \end{aligned}$$

where L is the maximum order of expansion and depends on the complexity of the phase function, $\mathbf{Z}^{c,m}(\mu, \mu')$ and $\mathbf{Z}^{s,m}(\mu, \mu')$ are computed by integrating the phase function with the cosine and sine

basis respectively. Similarly, we expand the vector radiance function in Fourier series as:

$$\mathbf{I}(\tau, \mu, \phi) = \frac{1}{2} \mathbf{I}^{c,0}(\tau, \mu) + \sum_{m=1}^L (\mathbf{I}^{c,m}(\tau, \mu) \cos m\phi + \mathbf{I}^{s,m}(\tau, \mu) \sin m\phi).$$

Using these expansions, we can write VRTE equation for the m -th order Fourier coefficients of \mathbf{I} as a pair for $m \geq 1$:

$$\begin{aligned} \mu \frac{\partial}{\partial \tau} \mathbf{I}_k^{c,m}(\tau, \mu) + \mathbf{I}_k^{c,m}(\tau, \mu) - \mathbf{J}_k^- &= \mathbf{Q}_k^{c,m}(\tau, \mu) \\ \mu \frac{\partial}{\partial \tau} \mathbf{I}_k^{s,m}(\tau, \mu) + \mathbf{I}_k^{s,m}(\tau, \mu) - \mathbf{J}_k^+ &= \mathbf{Q}_k^{s,m}(\tau, \mu) \end{aligned} \quad (15)$$

where the \mathbf{J}_k terms are defined as:

$$\begin{aligned} \mathbf{J}_k^- &= \frac{\omega(\tau)}{2} \sum_{l=-m}^L \int_{-1}^1 (\mathbf{Z}_l^{c,m}(\tau, \mu, \mu') \mathbf{I}_k^{c,m}(\tau, \mu') - \mathbf{Z}_l^{s,m}(\tau, \mu, \mu') \mathbf{I}_k^{s,m}(\tau, \mu')) d\mu', \\ \mathbf{J}_k^+ &= \frac{\omega(\tau)}{2} \sum_{l=-m}^L \int_{-1}^1 (\mathbf{Z}_l^{c,m}(\tau, \mu, \mu') \mathbf{I}_k^{c,m}(\tau, \mu') + \mathbf{Z}_l^{s,m}(\tau, \mu, \mu') \mathbf{I}_k^{s,m}(\tau, \mu')) d\mu', \end{aligned}$$

and the inhomogeneous terms \mathbf{Q}_k 's are defined as follows:

$$\begin{aligned} \mathbf{Q}_k^{c,m}(\tau, \mu) &= \frac{\omega(\tau)}{2} \sum_{l=m}^L \mathbf{Z}_l^{c,m}(\tau, \mu, \mu_{inc}) \mathbf{I}_{inc}(\mu_{inc}) e^{-\tau/\mu_{inc}}, \\ \mathbf{Q}_k^{s,m}(\tau, \mu) &= \frac{\omega(\tau)}{2} \sum_{l=m}^L \mathbf{Z}_l^{s,m}(\tau, \mu, \mu_{inc}) \mathbf{I}_{inc}(\mu_{inc}) e^{-\tau/\mu_{inc}}. \end{aligned}$$

To obtain the complete solution of the radiance field in the volume and at the boundary, we solve the collection of inhomogeneous equations defined by (15) for a specified boundary condition. The boundary conditions of our interest are as follows:

- No incident radiance at the top of the layer from any direction other than μ_{inc} , i.e. $\mathbf{I}_k^m(0, \mu) = \mathbf{0}$ for $\mu \leq 0$ and $\mu \neq \mu_{inc}$.
- For the material layer placed on the top of a black-body base, there is no entering radiance from the bottom of the layer. i.e. $\mathbf{I}_k^m(\tau_0, \mu) = \mathbf{0}$ where τ_0 is the thickness of the material layer, and $\mu > 0$. For the material layer placed on the top of a reflector, $\mathbf{I}_k^m(\tau_0, \mu)$ must be computed by integrating the known BRDF of the base reflector with $-\mu' \mathbf{I}_k^m(\tau_0, \mu')$ where $\mu' < 0$.

We use a discrete ordinate based method (DOM) for solving the inhomogeneous equations. Following the standard practice in DOM solutions, we assume a layer of the plane parallel medium to be homogeneous, that means the phase function, scattering and absorption coefficients and the single scattering albedo are constants in the layer (i.e. independent of τ inside the layer), and the optical thickness in a layer is simply the product of actual thickness in the layer and its extinction coefficient. We model the inhomogeneity of the material by decomposing the plane-parallel medium by multiple layers of homogeneous media (see figure 3). We refer the reader to previous work from Thomas and Stamnes [13] for more details on a DOM based solution method.

3.6 Computing Mueller Matrix for Subsurface BRDF

The Mueller matrix of the polarimetric BRDF (\mathbf{F}_r) must satisfy the following relation:

$$\mathbf{F}_r(\mu, \mu_{inc}, \phi - \phi_{inc}) \mathbf{E}_{inc}(\mu_{inc}) = \mathbf{I}(0, \mu, \phi), \quad (16)$$

where \mathbf{E}_{inc} is the irradiance incident from direction (μ_{inc}, ϕ_{inc}) , and $\mathbf{I}(0, \mu, \phi)$ is the radiance due to subsurface scattering at the surface (i.e. $\tau=0$) of the material.

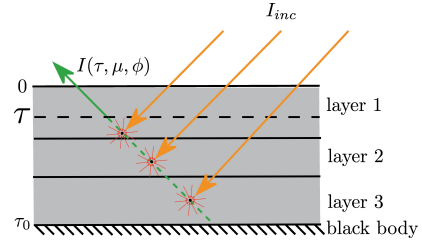


Figure 3: Material composed of three plane-parallel layers. The computation of the radiance at an optical thickness of τ in a direction (μ, ϕ) requires solving RTE for each layer. It involves the computation of the scattered radiance along (μ', ϕ') from all direction (small arrows) and the scattering of the attenuated incident radiance (long arrows).

We compute this matrix by computing radiance field for four linearly independent irradiance Stokes vectors, for every incident direction, and using the following relation:

$$\mathbf{F}_r(\mu, \mu_{inc}, \phi - \phi_{inc}) = [\mathbf{I}^{(1)}(0, \mu, \phi), \dots, \mathbf{I}^{(4)}(0, \mu, \phi)] \times [\mathbf{E}_{inc}^{(1)}(\mu_{inc}), \dots, \mathbf{E}_{inc}^{(4)}(\mu_{inc})]^{-1}. \quad (17)$$

We choose the following irradiance stokes vector values for our BRDF matrix computation:

$$\mathbf{E}_{inc}^{(1)} = \begin{bmatrix} 1 \\ 0 \\ 0 \\ 0 \end{bmatrix}, \quad \mathbf{E}_{inc}^{(2)} = \begin{bmatrix} 1 \\ 1 \\ 0 \\ 0 \end{bmatrix}, \quad \mathbf{E}_{inc}^{(3)} = \begin{bmatrix} 1 \\ 0 \\ 1 \\ 0 \end{bmatrix}, \quad \mathbf{E}_{inc}^{(4)} = \begin{bmatrix} 1 \\ 0 \\ 0 \\ 1 \end{bmatrix}.$$

The inverse matrix for (17) for this set of irradiance vectors is:

$$\begin{bmatrix} 1 & -1 & -1 & -1 \\ 0 & 1 & 0 & 0 \\ 0 & 0 & 1 & 0 \\ 0 & 0 & 0 & 1 \end{bmatrix}. \quad (18)$$

We compute the BRDF matrices by solving the VRTE for each of these four incident irradiance stokes vectors for each incident direction. Note that parts of the solution are independent of the incident direction and therefore do not need to be repeated four times. The resulting BRDF matrices are expressed in their reference frames following the definition in section 3.2, i.e. in reference to a meridional plane containing the direction and the vertical axis Z . As we assumed our material to be composed of horizontal layers, when applied to a scene for rendering, the meridional plane becomes the one containing the direction and the normal at the surface.

4 IMPLEMENTATION, VALIDATION AND RESULTS

We implemented our VRTE solver using C++ and the EIGEN library [1]. This solver takes the following input: the incident irradiance vector, a set of incident zenith angles, a set of outgoing azimuth and zenith angles defining the radiance field directions, the bottom boundary condition, and finally the number of layers, and information for each layer: layer optical thicknesses and material information. The solver accepts phase function coefficients and single scattering albedo of the layer as input material information. The solver outputs the Mueller matrix for the polarized BRDF for each pair of incident and outgoing direction, and optionally outputs the polarized radiance field at the specified optical thickness for each incident direction. The latter is used mostly for validation purposes. The tabulated BRDF were then used for renderings using our own polarized ray tracer written in OpenCL [19, 20].

We compute the Fourier expansion coefficients for equation 14 using the analytic expansion from [12]:

$$\mathbf{Z}^{c,m}(\mu, \mu') = \mathbf{A}^m(\mu, \mu') + \mathbf{D}\mathbf{A}^m(\mu, \mu')\mathbf{D}, \quad (19)$$

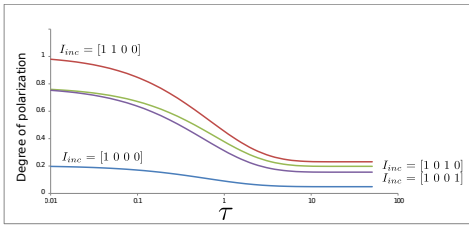


Figure 4: Degree of polarization as function of the optical thickness of the layer. From top to bottom, the incident light is horizontally polarized ($I_{inc} = [1 1 0 0]$), polarized along 45 degrees ($I_{inc} = [1 0 1 0]$), circularly polarized ($I_{inc} = [1 0 0 1]$) and unpolarized ($I_{inc} = [1 0 0 0]$)

$$\mathbf{Z}^{s,m}(\mu, \mu') = \mathbf{A}^m(\mu, \mu')\mathbf{D} - \mathbf{D}\mathbf{A}^m(\mu, \mu'), \quad (20)$$

$$\mathbf{A}^m(\mu, \mu') = \sum_{l=m}^L \mathbf{P}_l^m(\mu)\mathbf{B}_l\mathbf{P}_l^m(\mu'). \quad (21)$$

\mathbf{D} in the equations is the diagonal matrix $\text{diag}\{1, 1, -1, -1\}$, and \mathbf{B}_l defines the scattering property of the medium in matrix:

$$\mathbf{B}_l = \begin{bmatrix} \beta_l & \gamma & 0 & 0 \\ \gamma & \alpha_l & 0 & 0 \\ 0 & 0 & \zeta_l & -\varepsilon_l \\ 0 & 0 & \varepsilon_l & \delta_l \end{bmatrix}. \quad (22)$$

where β , α , ζ , δ , γ , and ε are the coefficients of expansion of the functions $a_1(\Theta)$, $a_2(\Theta)$, $a_3(\Theta)$, $a_4(\Theta)$, $b_1(\Theta)$, and $b_2(\Theta)$ from equation 10, and are computed using Mie theory. \mathbf{P}_l^m is a 4×4 matrix composed of the normalized associated Legendre polynomials P_l^m and generalized spherical polynomials $P_{m,n}^l$ [11]:

$$\mathbf{P}_l^m(\mu) = \begin{bmatrix} P_l^m(\mu) & 0 & 0 & 0 \\ 0 & R_l^m(\mu) & -T_l^m(\mu) & 0 \\ 0 & -T_l^m(\mu) & R_l^m(\mu) & 0 \\ 0 & 0 & 0 & P_l^m(\mu) \end{bmatrix}, \quad (23)$$

with R_l^m and T_l^m defined as:

$$R_l^m(\mu) = -\frac{1}{2}(i)^m[P_{m,2}^l(\mu) + P_{m,-2}^l(\mu)],$$

$$T_l^m(\mu) = -\frac{1}{2}(i)^m[P_{m,2}^l(\mu) - P_{m,-2}^l(\mu)].$$

For computing scattering coefficients using Mie theory, we use wavelength dependent refractive index data from publicly available SOPRA [3] and filmetrics [2] optical databases. The refractive indices used for our results can be found in table 2. Our implementation supports three types of base materials: a black body (no light is reflected from the bottom), a depolarizing Lambertian surface and a metallic surface whose reflection is modeled by the Fresnel equation. Figure 9 shows the rendering of a single layer of material composed of rust particles on top of those three base layers.

4.1 Validation

For validation, we applied our solver to the problem specified in the benchmark from Wauben and Hovenier [15]. This benchmark tabulates the polarized radiance field for several plane-parallel media illuminated by an unpolarized incident light source from direction ($\mu_{inc} = -0.6, \phi_{inc} = 0$). Figure 5 shows the plot of the first two elements of the Stokes vectors at two different τ values for the problem #2 of the benchmark, as a function of μ at $\phi = 0$. The results from our solver (continuous curves) are in perfect agreement with the

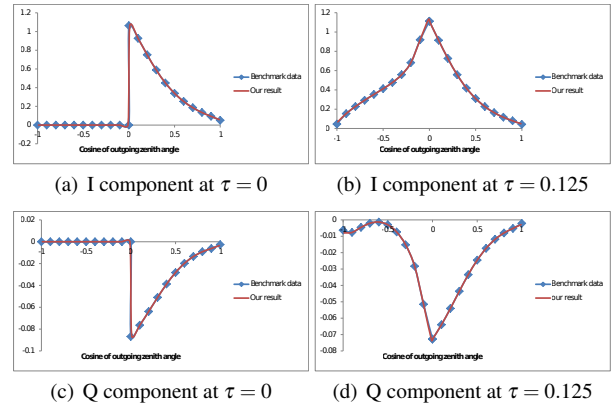


Figure 5: Comparison between our results (continuous curves) and the tabulated data from Wauben and Hovenier benchmark [15] (dots). We plot the I and Q elements of the radiance Stokes vector.

tabulated values from the benchmark (dots). The radiance field at $\tau = 0$ for negative μ values are zero because the incident field is zero (except for $\mu = \mu_{inc}$) at the top boundary.

In order to validate our BRDF computation approach from section 3.6, we used our solver to compute the radiance field for five different incident vectors. We used four of them to compute the BRDF matrix, and verified that multiplying that matrix with the fifth incident vector would give the same result as our solver. The results matched for all the outgoing directions.

4.2 Experimental Evidence of Polarizing Subsurface reflection

Preliminary tests with our solver indicated that the reflected radiance field due to subsurface scattering could exhibit polarization, particularly for thin layers of materials. We verified this finding through measurements of reflection from a thin layer of paint. For this experiment, we applied a thin layer of metallic car paint (Naple Gold Metallic YR524M Honda) on the top of a chromium metal disc. For our incident light, we used a vertically polarized laser beam from a Helium-Neon laser device. The beam is then passed through a half-wave plate. This arrangement allowed us to rotate the plane of polarization of the beam. The resulting beam then hits the paint surface. A narrow beam of the reflected light is passed through a beam splitter to separate the horizontally polarized and vertically polarized components of the reflected light. The separated components are measured through a light meter. Figure 6 summarizes the setup of the measurement. This setup allowed us to measure only the proportion of horizontal and vertical polarization components of the reflected field. After completing the measurement for a number of polarization states of the incident light, we added liberal amounts of the paint on the top of the sample to create a very thick layer, and repeated similar measurements. We subtracted the light meter readings for reflection from the thick layer, from the reading of the thin layer. Assuming that the final thick layer contributed negligible polarizing effect due to subsurface reflection, this latter step was carried out to remove the polarizing effect due to the surface reflection. Our results are shown in table 1. The reflected value for all measurements exhibited polarization. The ratio between the horizontal and vertical components of the measurements correlated with the ratio of the incident light, but were never the same. To compare the measurement with the result from our solver, we carried out an equivalent simulation. Note that

Input Incident light		Measured Reflected light		Finding from Simulation	
Horizontal	Vertical	Horizontal	Vertical	Horizontal	Vertical
0%	100%	11%	89%	28%	72%
7%	93%	19%	81%	32%	68%
25%	75%	24%	76%	41%	59%
50%	50%	37%	63%	54%	46%
75%	25%	63%	37%	66%	34%
93%	7%	98%	2%	74%	26%
100%	0%	86%	14%	77%	23%

Table 1: Percentage of horizontal and vertical linear polarization after reflection of different polarized incident light. The first two columns correspond to the percentage of horizontally and vertically polarized light of the incident beams. Columns 3 to 4 are the same percentages for the reflection from a thin layer of paint from the measurement. The final two columns show the results obtained from our solver for a simulated reflection from a layer of paint containing thin layer of aluminum particles (0.5 optical thickness) placed on the top of chromium metal. The incident stokes vector and the wavelength for the measurement and for the simulation are kept same.

the content of the actual paint material was entirely unknown. As a best guess we used a thin layer of material containing aluminum particles over chromium metal base. The Stokes vector for the incident light were computed to match exactly with the experiment input. The result of the simulation (the rightmost column of the table) showed a reasonably good agreement with our measured observation.

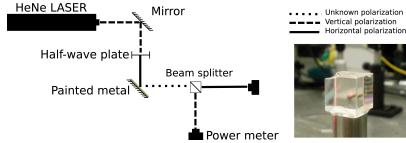


Figure 6: Schematic of our experimental setup. The vertically polarized light beam exiting the laser goes through the half-wave plate to let us control the angle of polarization, reflects on the painted metal and passes through the beam splitter to separate the vertically (red beam) and horizontally (green beam) polarized components of reflection and are each measured using a power meter. The image on the right is the picture of the beam splitter.

4.3 Comparison of BRDF computed using RTE and VRTE solver

Subsurface light transport involves scattering of light, modeled through the phase matrix, and each scattering event changes the polarization properties of the scattered light. Scalar computations omit these changes, and thus introduce errors into the computed radiance field and hence into the computed BRDF. To demonstrate this, we computed subsurface BRDF for different materials both with and without polarization properties, and computed the error

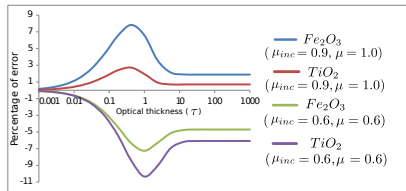


Figure 7: Percentage of error between scalar and polarized computations as a function of optical thickness of the layer. Each curve corresponds to a different pair of incident and outgoing angles (μ_{inc}, μ). The first and third curves (from top to bottom) are for layers of Iron oxide with angles (0.9, 1.0) and (0.6, 0.6) respectively. The other two curves correspond to titanium dioxide particles for the same direction pairs.

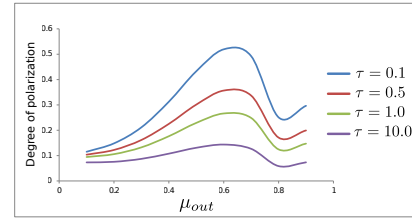


Figure 8: Degree of Polarization as a function of the outgoing angle μ . Each curve corresponds to a layer of Titanium dioxide particles with different optical thicknesses τ .

between the two results. For this error computation, we used the top left element of the computed BRDF matrix. In the subsequent text, we refer to it as F_v , and BRDF from scalar computation as F_s . The error $e = 1 - \frac{F_s}{F_v}$ depends on several factors, such as the material, the wavelength, the incident and reflected directions, and the thickness of the material. The figure 7 plots e for material layers composed of titanium dioxide particles and iron oxide particles and various layer thicknesses. The radius of the particles used is set at $0.2\mu m$, which is the size that the manufacturer try to maintain in titanium dioxide based paints for optimal light reflection. We can see from the plot that for very thin layers (optical thickness below 0.001), e is negligible, but it increases to a maximum of 11% (for a layer of titanium dioxide at optical thickness around 1.0) and remains relatively high (ex: 7% for layers of titanium dioxide at larger thicknesses) for certain incident angles.

4.4 Polarizing properties of BRDF

In this section we show how the polarization of the radiance field and hence the polarization properties of BRDF varies as a function of thickness of the pigment layer and the type of pigment. Figure 8 plots the degree of polarization of light after reflection of the light ray on a layer of titanium dioxide paint as a function of the outgoing μ direction.

Thus we demonstrated that, scalar computations lead to approximations, and accounting for polarized interaction of light is essential for accurate BRDF computation.

For this plot we used $0.2\mu m$ as the particle size. The reflected radiance was computed for $\mu_{inc} = -0.6$, and each curve corresponds to a different optical thickness. As expected, the curves show that the degree of polarization reduces with the thickness of the paint layer. Indeed, the thicker a layer, the more subsurface scattering events occur, randomizing more and more the polarization state of light. However in this example case, the degree of polarization was never less than 5% even for the thickest paint layer. Figure 10 shows a rendering of 4 spheres covered with those same layers of paint,

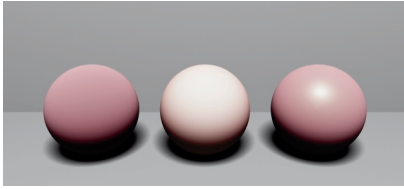


Figure 9: Rendering of a layer of rust particles over a black-body sphere (left), a white sphere (middle) and a silver sphere (right). Rust particles have a size of $0.2\mu m$ and the layer has an optical thickness of 1.

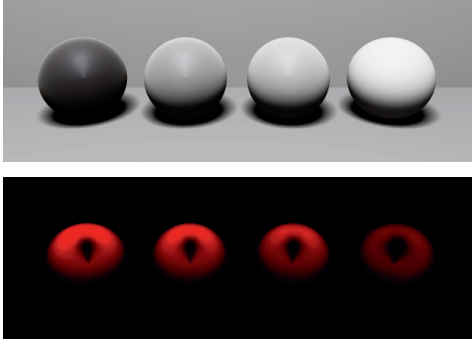


Figure 10: Rendering of spheres covered with a layer of Titanium dioxide paint. The optical thickness of the paint layers are (from left to right): 0.1, 0.5, 1.0 and 10.0. The bottom image shows the corresponding degree of polarization.

with increasing thickness from right to left. At the top we can see the resulting image while the bottom image shows the degree of polarization. We use here the visualization technique suggested by Wilkie et al. [17]. The more red a pixel, the stronger the degree of polarization of the light received by the camera through that pixel. Once again, we see that the thicker the material, the less is the degree of polarization. The walls and floor used in the rendering act as depolarizer and therefore do not have any polarization.

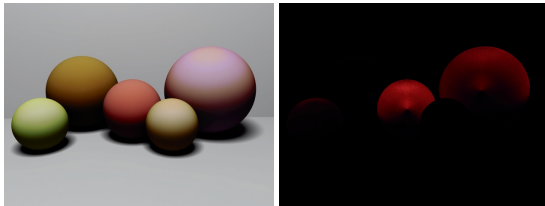


Figure 11: Rendering of spheres with different paints (on the left) and corresponding degree of polarization (on the right).

The degree of polarization is a function of optical thickness and the type of particles that compose the paint. Figure 11 shows several spheres painted with different materials, as well as the associated degree of polarization. From left to right, the paints used were aluminium gallium arsenide over a white depolarizing surface, thick layer of gold paint, thick layer of rust particles, gold paint over white depolarizing surface, and rust over a white depolarizing surface. All the particles composing the paints used here have a size of $0.2\mu m$. We can see that polarization differs between the materials as some spheres present important polarization effects while the others show very little.

In figure 8, we show that relatively thick layers, which are more likely to be seen in real life, are responsible for some but not much

polarization. It does not mean however that they act as depolarizer. Figure 4 shows the DOP of light reflected on the same titanium dioxide paint as a function of the optical thickness τ . Each curve

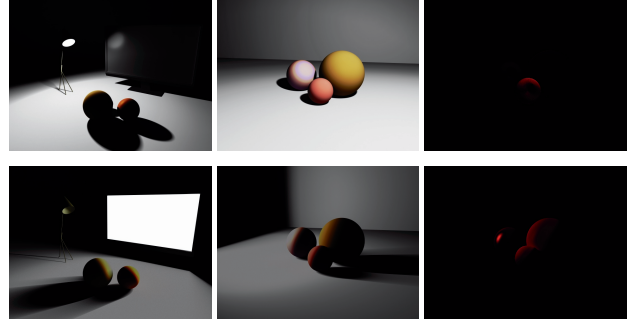


Figure 12: Rendering of a scene with different light sources. Images on the top row were rendered using a desk lamp as an unpolarized light source. Images at the bottom row have a monitor as a right circularly polarized light source. The first column gives a global view of the scene and the last two columns show the rendering of the spheres and the associated degree of polarization.

corresponds to incident light at a different state of polarization (unpolarized, horizontal and vertical linear polarization and right circular polarization). While those states may not correspond to real-life light sources, it permits us to see how the material affects an already polarized light. As in the previous case, the unpolarized light sees its DOP decrease as the material gets thicker, but when considering fully polarized incident light, the degree of polarization never goes below 20% after reflection even for layers with an infinite optical thickness. Figure 12 shows a scene illuminated by a desk lamp casting unpolarized light, and a computer screen casting circularly polarized light. The figure shows the rendering and the associated degree of polarization using these sources. Though little polarization is present when the light source is the desk lamp, all the three spheres exhibit polarization when the monitor screen is used, thus showing that even materials not creating polarization can convey important polarization information in global illumination.

Material	450nm		550nm		650nm	
	n	k	n	k	n	k
TiO_2	3.141	0.000	2.954	0.000	2.860	0.000
Gold	1.509	1.879	0.350	2.714	0.168	3.118
Iron oxide	0.253	0.692	0.260	0.383	0.023	0.218
$AlGaAs$	3.832	0.183	3.411	0.000	3.239	0.000
Silver	0.151	2.470	0.125	3.339	0.139	4.129

Table 2: Real and complex components of the refractive indices of the particles used in this paper

Figure 13 shows the BRDF lobes for paint layers composed of different materials. Each paint layer was placed on top of three different base layers: black body, a white depolarizing Lambertian surface and a metallic silver base acting as a polarizing mirror. The BRDF of the paint layers exhibited similar trends. The Lambertian base made the BRDF lobe bigger (visible on the first row), but reduced the degree of polarization of the reflected light significantly (shown on the second row). Using silver base however not only increased the BRDF, but also created a lobe along the mirrored light direction, adding to the material specular effect. Metallic bases plays also a big role on polarization as they clearly change the shape of the degree of polarization lobe as seen on the second row. The rendering of each BRDF applied to a statuette using an environment map is shown on the last row of (13) and agree with the previous observations. Middle rendering are more pale than the

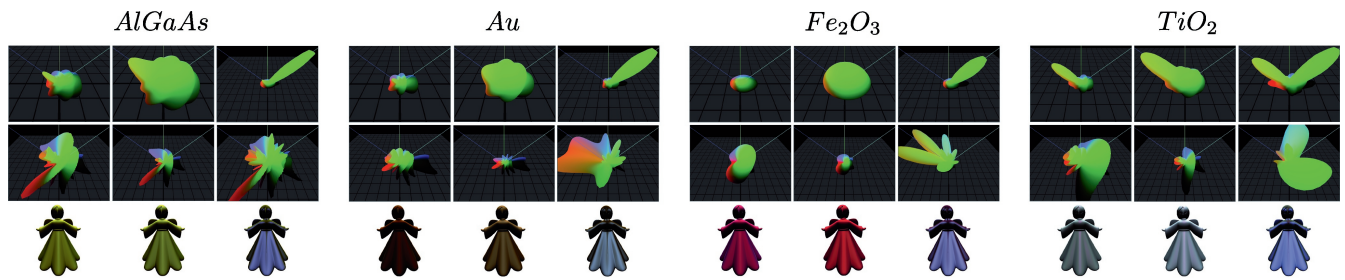


Figure 13: BRDF lobes for different materials. The first row shows the BRDF lobe, the second shows degree of polarization of the reflected unpolarized incident light and the third row shows the rendering of the BRDF applied on a statuette using an environment map. The optical thickness of the layers are kept at 1.0, and the particle size at $0.6\mu\text{m}$. For each particle type, the first column corresponds to the layer on top of a black body, the middle column is for the layer on top of a white depolarizing Lambertian surface, and the right column is on top of a metallic Silver base. The lobes correspond to an incident light coming from the top left corner, with an inclination of 45° . AlGaAs lobe is shown for a wavelength of 550nm while the others are for a wavelength of 650nm .

left ones, because of the white base, while most of the color on the right side renderings come from the reflection of the environment map itself. A rendering of a statuette with a visible environment map is shown on figure 14.

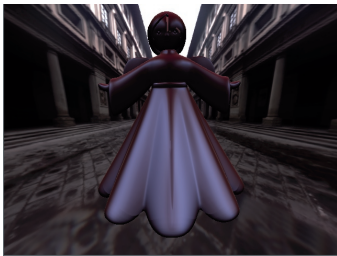


Figure 14: Rendering of an Angel Statuette using a material composed of a layer of iron oxide particles on top of a silver base. The environment map used corresponds to Florence's Uffizi gallery.

5 CONCLUSION AND FUTURE WORK

Light transport during subsurface interaction involves multiple changes of the polarization state of the light, which depends on the types of pigment particles that make up the subsurface medium. Though the polarization properties are not visually important, they are needed for accurate computation of light transport, and hence must be accounted for in the BRDF computation and in global illumination computation.

We described vector radiative transport equation (VRTE) for modeling polarizing light interaction in media. We described a discrete ordinate based method for solving VRTE and used it to compute BRDF due to subsurface interaction of light.

Our VRTE solver, though complete, is slow. Depending on the complexity of the scattering medium, a single BRDF computation for $51 \times 51 \times 61$ directions takes 5 to 10 minutes. We are working towards parallelizing the computation steps and porting to GPU to speed up the computation.

Our preliminary experimental study supports the polarizing behavior of the subsurface BRDF. In future we would like to improve our experimental setup, to support both polarized and unpolarized input, to make full Stokes measurements and to measure the full reflection field. This will allow us to make full scale validations and better understand some of the observed optical behavior.

ACKNOWLEDGEMENTS

This work was supported by NSF grant IIS-1064427. Environment maps were taken from University of Southern Cali-

fornia high-resolution light probe image gallery.

REFERENCES

- [1] Eigen library: <http://eigen.tuxfamily.org>.
- [2] Filmetrics: <http://filmetrics.com/>.
- [3] Sopra: <http://www.spectra.com/sopra.html>.
- [4] M. Bass, E. W. Van Stryland, D. R. Williams, and W. L. Wolfe. *Handbook of optics*, volume 2. McGraw-Hill, 2001.
- [5] S. Chandrasekhar. *Radiative transfer*. Dover publications, 1960.
- [6] J. Dorsey, H. Rushmeier, and F. Sillion. *Digital Modeling of Material Appearance*. Morgan Kaufmann Publishers Inc., San Francisco, CA, USA, 2008.
- [7] P. Hanrahan and W. Krueger. Reflection from layered surfaces due to subsurface scattering. In *Proceedings of the 20th annual conference on Computer graphics and interactive techniques, SIGGRAPH '93*, pages 165–174, New York, NY, USA, 1993. ACM.
- [8] E. Hecht and A. Zajac. *Optics*, volume 4. Addison Wesley San Francisco, CA, 2002.
- [9] J. Hovenier and C. Van der Mee. Fundamental relationships relevant to the transfer of polarized light in a scattering atmosphere. *Astronomy and Astrophysics*, 128:1–16, 1983.
- [10] H. W. Jensen, S. R. Marschner, M. Levoy, and P. Hanrahan. A practical model for subsurface light transport. In *Proceedings of the 28th annual conference on Computer graphics and interactive techniques*, pages 511–518. ACM, 2001.
- [11] C. Siewert. On the equation of the transfer relevant to the scattering of polarized light. *The Astrophysical Journal*, 245:1080–1086, 1981.
- [12] C. Siewert. A discrete-ordinates solution for radiative-transfer models that include polarization effects. *Journal of Quantitative Spectroscopy and Radiative Transfer*, 64(3):227 – 254, 2000.
- [13] G. E. Thomas and K. Stamnes. *Radiative transfer in the atmosphere and ocean (Chapter 8)*. Cambridge University Press, 2002.
- [14] K. E. Torrance and E. M. Sparrow. Theory for off-specular reflection from roughened surfaces. *JOSA*, 57(9):1105–1112, 1967.
- [15] W. Wauben and J. Hovenier. Polarized radiation of an atmosphere containing randomly-oriented spheroids. *Journal of Quantitative Spectroscopy and Radiative Transfer*, 47(6):491 – 504, 1992.
- [16] A. Wilkie, R. Tobler, C. Ulbricht, G. Zotti, and W. Purgathofer. An analytical model for skylight polarisation. In *Eurographics Symposium on Rendering*, volume 25, pages 53–69. Citeseer, 2004.
- [17] A. Wilkie and A. Weidlich. A standardised polarisation visualisation for images. In *Proceedings of the 26th Spring Conference on Computer Graphics*, pages 43–50. ACM, 2010.
- [18] A. Wilkie and A. Weidlich. How to write a polarisation ray tracer. In *SIGGRAPH Asia 2011 Courses*, page 8. ACM, 2011.
- [19] A. Wilkie, A. Weidlich, and A. Ghosh. Polarised light in computer graphics. In *SIGGRAPH Asia 2012 Courses*, page 8. ACM, 2012.
- [20] L. B. Wolff and D. J. Kurlander. Ray tracing with polarization parameters. *Computer Graphics and Applications, IEEE*, 10(6):44–55, 1990.